Nuclear Materials and Energy 16 (2018) 238–244

Contents lists available at ScienceDirect

Nuclear Materials and Energy

journal homepage: www.elsevier.com/locate/nme

First principles study of point defect effects on iodine diffusion in zirconium

Rui Tu[a], Qin Liu[a], Cheng Zeng[c], Yingying Li[a,b], Wei Xiao[*,a,b]

[a] Division of nuclear materials and fuel, State Power Investment Corporation Research Institute, Beijing 102209, PR China
[b] National Energy R&D Center of Nuclear Grade Zirconium Materials, Beijing 102209, PR China
[c] School of Engineering, Brown University, Providence, RI 02912, USA

ARTICLE INFO

Keywords:
Diffusion
Iodine
Zirconium
Point defects
First-principles calculations
Nudged elastic band method

ABSTRACT

The formation energies, diffusion barriers, and vibration frequencies of complex iodine defects in zirconium are calculated with first principles calculations and nudged elastic band method. The effective diffusion rates of these complex defects are evaluated in the temperature range from 300 K to 2000 K. The iodine interstitial diffusion and the iodine diffusion via $I_{Zr} - V_{Zr}$ are the dominant diffusion mechanisms. The vacancies may be traps for iodine diffusion and they can slow down the diffusion of iodine atoms. For the zirconium cladding materials in light water reactors, various point defects may be generated. Our calculated effective diffusion coefficients agree with the experimental data well and it indicates that bulk diffusion may be a main diffusion mechanism for the iodine diffusion in zirconium alloy.

1. Introduction

The fuel cladding material in the light water reactor (LWR) is an important safety barrier which is used to prevent the radioactive fuel products from releasing to the cooling water [1]. How radioactive fuel products release from the cladding materials is of great interests to engineers and researchers to develop high quality cladding materials [2].

One important fission product in LWR is radioactive iodine. For example, iodine isotopes ^{129}I ($T_{1/2}$ = 15.7 × 10^6 years) and ^{131}I ($T_{1/2}$ = 8 days) in the thyroid gland is harmful to human body [3,4]. In light water reactors, iodine induced stress corrosion cracking (ISCC) occurs on the inner side of the zirconium fuel cladding [5–7]. As a result, the diffusion of iodine in zirconium alloy is an interesting topic. Diffusion of various fission products in cladding materials have been studied with experimental methods [8–14]. For example, ion implantation method is used to generate iodine impurity in cladding materials, and following high temperature annealing is used to activate the diffusion process, then, Rutherford back scattering spectrometry (RBS) is used to detect the concentration and analyze the diffusion for the iodine diffusion in Zr [8] and SiC [10–12].

Computational simulations are also used to study the iodine in cladding materials [15–21]. They provide insights for material design and overcome the limitation of the experimental study. For example, irradiation facilities are expensive and the accuracy of the detection method is limited. Diffusion of Cs, Ag, and B in silicon carbide have been studied by Morgan et al. [22–27]. Trinkle and his co-authors studied oxygen diffusion in various *hcp* metals, including zirconium [28,29]. Interstitial iodine diffusion in a stoichiometric SiC sample is calculated and compared with the diffusion of iodine interstitial in zirconium by first principles calculation and nudged elastic band methods [30]. Since neutron irradiation will generate various point defects in the cladding material, defect effects on iodine diffusion in zirconium is an important topic [31–34].

In this paper, first-principles calculations [15,35] and nudged elastic band (NEB) method [36–38] are used to study the formation energies, migration energy barriers, and attempt-to-diffuse rates of various iodine defects in bulk zirconium material. Effective energy barriers and attempt-to-diffuse rates can be used to analyze the differences among different diffusion mechanism [22,23] and they are calculated for iodine diffusion via different point defects.

2. Calculation methods

2.1. Density functional theory calculations

In the diffusion calculations, density functional theory (DFT) calculations [15,35] are performed to calculate the system energies with Vienna *ab initio* Simulation Package(VASP) code [39–41]. Projected augmented wave (PAW) method [42,43] is used to deal with the wave functions near the core region of atoms and the exchange correlation functional within the generalized gradient approximation (GGA)

* Corresponding author at: Division of nuclear materials and fuel, State Power Investment Corporation Research Institute, Beijing 102209, PR China.
E-mail addresses: xiaowei1@gmail.com, xiaowei@snptc.com.cn (W. Xiao).

https://doi.org/10.1016/j.nme.2018.07.006
Received 28 March 2018; Received in revised form 11 July 2018; Accepted 13 July 2018
Available online 29 July 2018
2352-1791/ © 2018 The Authors. Published by Elsevier Ltd. This is an open access article under the CC BY-NC-ND license (http://creativecommons.org/licenses/BY-NC-ND/4.0/).

parameterized by Perdew, Burke, and Enzerof (PBE) [44,45] is used in the calculations. The cutoff of the plane-wave kinetic energy is 350 eV. The spin polarization is used in all calculations. The residual minimization method with direct inversion in the iterative subspace (RMM-DIIS) [46,47] is used in the electronic relaxation and the energy convergence criterion is 10^{-4} eV. Conjugate gradient method is used to minimize the Hellmann–Feynman forces in the ionic relaxations and the force stopping criterion is 0.05 eV/Å. A $6 \times 6 \times 3$ super cell with 216 Zr atoms is fully relaxed and then it is used for the formation energy calculation. During the defect formation energy calculations, the box size is fixed and the atoms inside are relaxed. The summations over the Brillouin zone are performed with a $2 \times 2 \times 2$ Monkhorst–Pack k-point mesh.

2.2. Formation energy of a point defect

Since point defect may affect the diffusion of iodine atom in bulk zirconium, various point defects are generated in the zirconium super cell. The formation energy (F) of certain point defect in a zirconium super cell is defined as the following equation [48],

$$\begin{aligned} F &= E^r - E_{pure} + \Sigma dn_s E_s \\ &= E^r - E_{pure} + dn_{Zr} E_{Zr} - E_I. \end{aligned} \tag{1}$$

Here, F represents the formation energy of certain point defect; E^r represents the energy of a structure which contains certain defect; E_{pure} is the system energy of the zirconium super cell without any defect; E_s represents for the energy of certain single atom or the cohesive energy per atom of certain bulk material, for example, E_I is the energy of an iodine atom inside a box with same shape and volume as the zirconium super cell and E_{Zr} is the cohesive energy per atom of bulk zirconium; dn_s is the corresponding atom number change for the species s inside the super cell after the doping process.

2.3. Diffusion rate calculations

Climb image nudged elastic band (CI-NEB) method [36–38] is used to search the minimal energy paths and calculate the diffusion energy barriers of an iodine atom diffusion inside zirconium with certain point defect. VTST code [49] coupled with VASP package are employed to perform the NEB calculations. There are four or more images between the initial and the final configurations for the NEB calculations. The fictitious spring constant is 5.0 eV/Å^2 and the force convergence criteria is 0.05 eV/Å. The volume is fixed in NEB calculation since the volume change can be ignored during diffusion process.

The frequency of diffusion follows the Arrhenius law [50],

$$\Gamma = \Gamma_0 exp\left(-\frac{\Delta E}{k_B T}\right), \tag{2}$$

where ΔE represents the diffusion energy barrier and Γ_0 is the attempt-to-diffuse frequency. Considering the transition state theory (TST) [51,52] and the classical harmonic approximation, the attempt-to-diffuse frequency is $\Gamma_0 = n\nu$, where n is the number of equivalent diffusion paths and ν is,

$$\nu = \frac{\Pi_{i=1}^{3N} \nu_i}{\Pi_{i=1}^{3N-1} \nu_i'}, \tag{3}$$

ν_i and ν_i' represent the normal vibration models of initial state and transition state. There are $3N-1$ normal models at transition state because one of the frequencies is imaginary. N is the atom number.

Since NEB calculations need more computer resource, balancing the computing time and the accuracy, a $4 \times 4 \times 2$ super cell with 64 Zr atoms is used for the NEB calculations.

2.4. Effective diffusion coefficient

The effective diffusion coefficient corrected by defect's concentration ratio can be used to describe iodine diffusion in zirconium with various defect types [48,53]. Iodine diffusion in zirconium had been investigated with ion implantation and Rutherford back scattering spectrometry (RBS) analysis [8]. The ion implantation is used to generate iodine impurity in various types. After ion implantation, high temperature annealing are used to activate the diffusion process and RBS is used to detect the concentration of iodine in Zr. If there are vacancies near the iodine impurities, local quasi-chemical equilibrium will be established between the vacancies and iodine atoms quickly [54,55]. With this equilibrium assumption, the effective diffusion coefficient can be written as [48,53],

$$D_i^{eff} = D_i^{int} \frac{c_i}{\sum c_i}. \tag{4}$$

D_i^{eff} and D_i^{int} in Eq. (4)represent the effective and intrinsic diffusivity of certain diffusion mechanism via specified defect. The c_i represents the concentration of certain point defect in the zirconium sample. The diffusion coefficient obeys the Arrhenius relationship,

$$D = D_0 exp\left(-\frac{\Delta E}{k_B T}\right), \tag{5}$$

and the diffusivity D_0 can be written as [48],

$$D_0 = d^2 \Gamma_0 = d^2 n \nu. \tag{6}$$

Here, d represents the diffusion length. Γ_0 is the attempt-to-diffuse frequency of certain diffusion mechanism and it is defined in Eqs. (2) and (3).

The denominator of the concentration part in Eq. (4) is the summation of the concentrations of all types of defects. This concentration part represents the probability of an iodine atom passing through certain type of defect. The concentration of certain type of defect can be estimated by the formation energy of this type of defect,

$$c_i = A_0 exp\left(-\frac{F_i}{k_B T}\right). \tag{7}$$

F_i is the formation energy of the defect type i.

Then we substitute Eqs. (5)–(7) into Eq. (4). Since the pre-factor A_0 in numerator and denominator of the concentration component are canceled, we get the following result,

$$\nu_i^{eff} exp\left(-\frac{\Delta E_i^{eff}}{k_B T}\right) = \nu_i^{int} exp\left(-\frac{\Delta E_i^{int}}{k_B T}\right) \frac{exp\left(-\frac{F_i}{k_B T}\right)}{\Sigma exp\left(-\frac{F_i}{k_B T}\right)} \tag{8}$$

The formation energies F_i, intrinsic vibration models ν_i^{int}, and the diffusion energy barriers E_i^{int} can be calculated from *ab initio* simulations and NEB method. Then the effective vibration model ν_i^{eff} and diffusion energy barrier E_i^{eff} of certain defect can be evaluated via Eq. (8) within certain temperature range. E_i^{eff} is linear proportional to $E_i^{int} + F_i$.

3. Results and discussion

3.1. Formation energies of iodine defects

As a cladding material, various point defects are generated in zirconium by irradiation effects. The fission product iodine may diffuse into the cladding tube via pellet cladding interaction (PCI). Point defect effect may affect the diffusion rate of iodine in zirconium. In this work, four types of point defects associated with iodine impurities in zirconium are studied. They are iodine interstitial, substitutional interstitial, substitutions, and substitutions with vacancies. The schematics of these four types of point defects are shown in Fig. 1.

The schematic of an iodine interstitial is shown in Fig. 1(a). For the

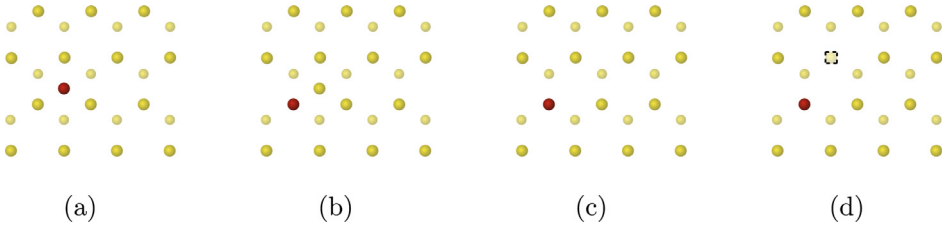

Fig. 1. Schematics of point defects associated with iodine atom in bulk zirconium (the direction out of the paper is ⟨001⟩). The yellow balls represent zirconium atoms. The red balls are the iodine atoms. The dash square represents a vacancy. (a) an interstitial iodine defect; (b) substitutional interstitial defect; (c) substitutional defect; (d) a substitutional iodine atom with a vacancy. (For interpretation of the references to colour in this figure legend, the reader is referred to the web version of this article.)

substitutional interstitial case, an iodine atom takes the position of a lattice zirconium atom and pushes the zirconium atom into a nearby interstitial site (see Fig. 1(b)). For a substitutional defect, an iodine atom takes the position of a zirconium atom and this intrinsic atom is kicked out (see Fig. 1(c)). Frenkel pairs are created during nuclear reactor operation by irradiation effect. The vacancies generated in this process may move close to the iodine atoms and affect the iodine diffusion. The schematic of a substitutional iodine atom with a vacancy nearby in bulk zirconium is shown in Fig. 1(d).

Since the substitutional interstitial is a type of interstitial, they are discussed in the subsection of interstitial below.

3.1.1. Iodine interstitial defects

Eight iodine interstitial sites in a zirconium unit cell are shown in Fig. 2. The tetrahedral (T) and octahedral (O) sites are two high symmetry interstitial sites. At these sites, an iodine interstitial atom has four or eight nearest Zr neighbor atoms. At a crowdion site (Crow), an iodine atom is surrounded by four nearest neighbor atoms. The formation energies for an iodine interstitial at the sites I_T, I_O, and I_C are 1.01 eV, 1.21 eV, and 1.13 eV, respectively.

All of the three type of interstitial sites have their corresponding basal sites, they are basal tetragonal center(BT) site, basal octahedral center (BO), and basal crowdian (BC) site. Among these configurations, only the BC site is stable, which has a formation energy of 1.21 eV.

If an interstitial iodine atom sharing a lattice site with a lattice zirconium atom, they form a split defect, or a dumbbell defect. There are two types of dumbbell configurations for this type of defect along different directions, for example, the dumbbell along ⟨001⟩ direction or ⟨100⟩ direction. They are named as S_z and S_x, respectively. The S_z site is not stable, and the defect S_x is stable with the formation energy of 1.20 eV.

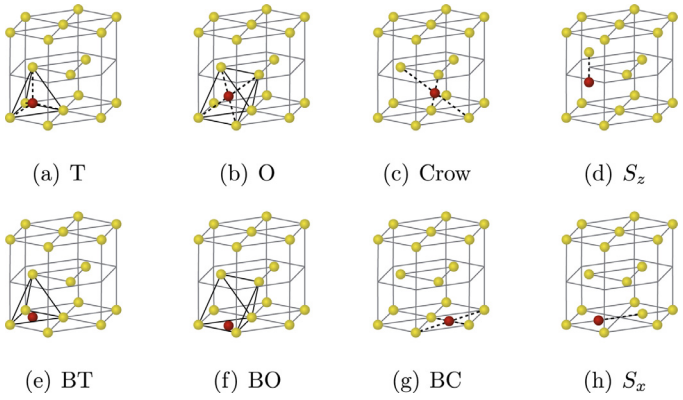

Fig. 2. Schematic of an iodine atom in bulk zirconium. The yellow balls represent zirconium atoms. The red balls are iodine atoms. The dash square represents a vacancy. (a) tetrahedral center; (b) octahedral center; (c) crowdion site; (d) split site along z direction; (e) basal tetrahedral center; (f) basal octahedral center; (g) basal crowdion site; (h) split along x direction. (For interpretation of the references to colour in this figure legend, the reader is referred to the web version of this article.)

Table 1
The formation energies (F) of iodine interstitial and sub-interstitial defects in Zr (eV).

Defects	F (eV)	Defects	F (eV)
I_{BC}	1.21	I_{Crow}	1.13
I_{BO}	Unstable	I_O	1.21
I_{BT}	Unstable	I_T	1.01
I_{S_x}	1.20	I_{S_z}	Unstable

In summary, I_T is the most stable interstitial defect. (Table 1)

3.1.2. Substitutional defects

If a zirconium atom is replaced by an iodine atom, a substitutional defect I_{Zr} is formed. The formation energy of I_{Zr} is − 0.73 eV.

3.1.3. Vacancy included defects

When zirconium cladding material works in water reactors, vacancies are generated in bulk zirconium by irradiation effects. Iodine diffusion may be affected by vacancies. The formation energies and the diffusion barriers of an iodine atom diffusion in zirconium with vacancies are calculated in this work. If there is a vacancy near an iodine substitutional atom, the notation of $I_{Zr} - V_{Zr}$ is used to describe this defect. The formation energies of various configurations of iodine impurity coupled with vacancies are listed in Table 2. In this table, the atom numbers of each element in the same row are the same for the different configurations. For example, in the first row, both of the defects $I_{Zr} - V_{Zr}$ (A-Type) and $I_{Zr} - V_{Zr}$ (B-Type) lose two lattice zirconium atoms and gain an extra iodine atom. The difference of these two defects is whether the impurity atom and the vacancy are in the same layer or not (See Fig. 3). The formation energies of these two defects are 0.89 eV and 0.83 eV respectively. It shows B-Type is energetically more stable than A-Type. Similarly, if the system has one more vacancy, three configurations are studied. They are $I_{2Zr} - V_{Zr}$, $I_{Zr} - 2V_{Zr}$, and $I_{Zr} - V_{Zr} - V_{Zr}$. In the configuration of $I_{2Zr} - V_{Zr}$, an iodine interstitial is at a divacancies site and there is another vacancy nearby; in the configuration of $I_{Zr} - 2V_{Zr}$, an iodine atom substitute a Zr atom with two vacancies which are in the same layer; in the configuration of $I_{Zr} - V_{Zr} - V_{Zr}$, an iodine atom substitute a Zr atom with two vacancies which are in different atomic layers. The formation energies of these three defects are 2.19 eV, 2.30 eV, and 2.33 eV respectively. So, $I_{2Zr} - V_{Zr}$ is more energetic favorable than the other two types (See Fig. 4).

The configurations with an iodine atom co-existing with more vacancies or other point defects are not considered in this work.

3.2. Diffusion of iodine in α−Zr with point defects

Point defects in α−Zr may affect the diffusion rate of an iodine atom in Zr. NEB method is used to search the minimal energy paths (MEP) of iodine diffusion processes in bulk zirconium and calculate the corresponding diffusion energy barriers via certain complex defects in this section. Since there are a lot of isomers for many types of defects, the configuration with the lowest formation energy for certain type of

Table 2
Formation energies F (eV) of an iodine impurity associated with vacancies.

	Defects	F	Defects	F	Defects	F
$Zr_{62}I_1$	$I_{Zr} - V_{Zr}$ (A-Type)	0.89	$I_{Zr} - V_{Zr}$ (B-Type)	0.83		
$Zr_{61}I_1$	$I_{2Zr} - V_{Zr}$	2.19	$I_{Zr} - 2V_{Zr}$	2.30	$I_{Zr} - V_{Zr} - V_{Zr}$	2.33

defect is considered to design the initial diffusion paths. For example, an iodine atom diffuses from a configuration with low energy to another symmetrical site. Since diffusion paths may be composed of several steps through several meta-stable configurations, the control steps of the diffusion paths are analyzed.

3.2.1. Intrinsic diffusion rate

The *intrinsic diffusion* rate is calculated with the diffusion energy barriers and vibration models directly from the first-principle calculation with NEB method without considering the concentration of certain defect. Since iodine diffusion in zirconium is not an isotropic process, two diffusion directions are considered. The inter layer diffusion is along the ⟨001⟩ direction, and the inner layer diffusion between two atomic layers is along ⟨100⟩ direction. The diffusion energy barriers and the vibration frequencies for each diffusion process are listed in Table. 3. The possible diffusion paths in the nearest neighbor of the impurity defect are investigated to find the control step of each diffusion mechanism and corresponding energy barrier. Since a diffusion path A may be composed of several steps, the energy barriers for all the diffusion steps are calculated with NEB method. The step with the highest barrier (ΔE_A) among these steps is the control step of this path and ΔE_A is the barrier for the whole path because this step is the bottleneck of the whole path. Suppose there is a parallel path B of which the barrier of its control step is ΔE_B, the path with the lower control barrier is energy favorable. For example, if $\Delta E_A < \Delta E_B$, the path A is energy favorable with the barrier of ΔE_A. After the calculation of various diffusion mechanisms, the diffusion barriers and corresponding attempt-to-diffuse frequencies of the control steps of them are listed in Table 3. The diffusion energy barriers of inner layer and inter layer diffusion are 0.14 eV and 0.24 eV, which are close to the former calculations of 0.16 eV and 0.23 eV [30].

Because the diffusion of $I_{Zr} - V_{Zr}$ is an important mechanism and it is relatively easy to describe compared with other mechanisms, it is described in detail as an example to demonstrate the MEP of the diffusion mechanism. The schematics of iodine diffusion via the defect of $I_{Zr} - V_{Zr}$ are shown in the Figs. 5 and 6. For the inter layer diffusion of an iodine via $I_{Zr} - V_{Zr}$, the iodine atom moves to the vacancy at the first step (see Fig. 5(a)). And then a neighbor zirconium atom moves to the vacancy or the original site of the iodine atom. In the third step, a zirconium atom at upper layer moves to the vacancy and forms a vacancy there until a symmetrical vacancy forms by at upper layer zirconium migration. Finally, the iodine atom and the corresponding vacancy move to a upper atomic layer. The final symmetrical configuration is shown in Fig. 5(e).

An iodine diffusion facilitated with a vacancy between two atomic layers ($I_{Zr} - V_{Zr}$) is schematically shown in Fig. 6. This path is composed of several serial diffusion steps, in which the one with the highest diffusion energy barrier is the control step of the whole path. The energy barrier and vibration frequency of the controlled step are listed in Table 3. For the intrinsic diffusion data, the diffusion barrier of the interstitial mechanism is the lowest and that of the substitutional mechanism is the highest. The diffusion energy barriers of the diffusion mechanisms via other defects are between these two situations.

Since HCP structure is not isotropic, the contributions from the inner and inter diffusion to the total diffusion coefficient are different. Due to the random nature of diffusion, the contribution from the inter diffusion ($D_{\|i}$, parallel to the $\vec{c}$ axis) and the inner diffusion ($D_{\perp i}$, perpendicular to the $\vec{c}$ axis) of the diffusion mechanism i to the total diffusion coefficient would be $\frac{1}{3}$ and $\frac{2}{3}$ respectively [54]. Then the total diffusion coefficient can be written as,

$$D_{tot} = \frac{1}{3}\sum_i D_{\|i} + \frac{2}{3}\sum_i D_{\perp i} \tag{9}$$

At 600 °C (873 K), our calculated diffusion coefficients of iodine interstitial, I_{Zr}, $I_{Zr} - V_{Zr}$, and $I_{2Zr} - V_{Zr}$ are $9.18 \times 10^{-9}\mathrm{m^2s^{-1}}$, $3.65 \times 10^{-27}\mathrm{m^2s^{-1}}$, $5.36 \times 10^{-11}\mathrm{m^2s^{-1}}$, and $7.77 \times 10^{-13}\mathrm{m^2s^{-1}}$ respectively. Comparing to the experimental data at the same temperature ($4.77 \times 10^{-17}\mathrm{m^2s^{-1}}$ [8]), the iodine diffusion via the mechanisms of interstitial, $I_{Zr} - V_{Zr}$, and $I_{2Zr} - V_{Zr}$ is faster than experimental data; on the other hand, iodine diffusion via I_{Zr} is much slower than the experimental data. It suggests that the experiment data is a combination of all possible diffusion mechanisms.

3.2.2. Effective diffusion coefficient

Because various point defects may be generated during the irradiation process, effective diffusion coefficients are calculated to evaluate their impacts on the diffusion of iodine. The effective diffusion coefficient of certain diffusion mechanism is proportional to the concentration of the corresponding point defect. Especially, the formation energies of the point defects and the diffusion barriers are at the same level for iodine defects in zirconium, both of the formation and the diffusion processes can be activated by thermal energy. Because the concentration of certain defect is determined by the corresponding formation energy (see Eq. (7)), the effective diffusion coefficient of

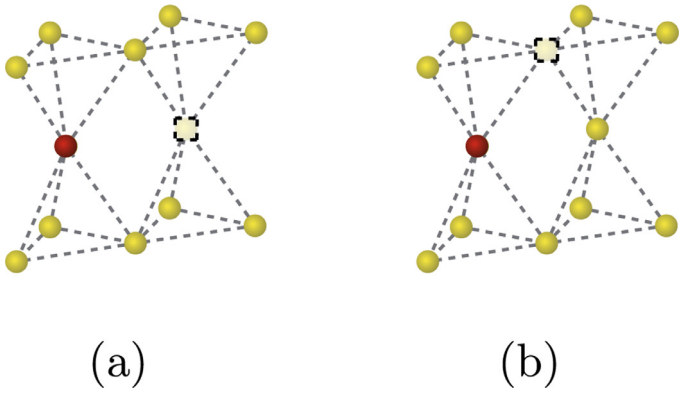

Fig. 3. Schematics of an iodine atom substitutes a zirconium atom with a vacancy nearby ($I_{Zr} - V_{Zr}$). The yellow balls are zirconium atoms and the red balls are iodine atoms. Dash-line square represents a zirconium vacancy. (a) in type A of $I_{Zr} - V_{Zr}$ (A-Type), the iodine atom and the vacancy are in the same layer; (b) in type B of $I_{Zr} - V_{Zr}$ (B-Type), that the iodine atom and the vacancy are in different layer. (For interpretation of the references to colour in this figure legend, the reader is referred to the web version of this article.)

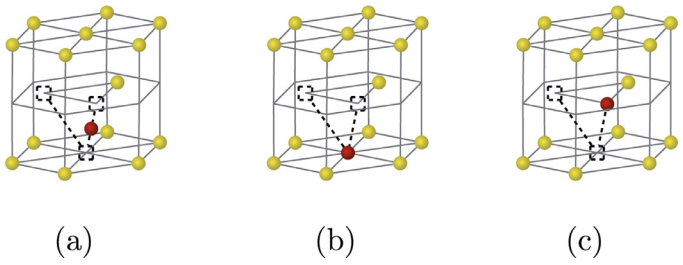

Fig. 4. Schematic of three isomers of iodine impurity with two vacancies in bulk Zr. Yellow balls represent Zr atoms. The red balls are iodine atoms. The dash square represents a vacancy. (a) an iodine interstitial atom is at a divacancies and there is another vacancy nearby; (b) an iodine atom substitutes a Zr atom and there are two vacancies nearby which are in the same atomic layer; (c) an iodine atom substitutes a Zr atom and there are two vacancies nearby which are in different atomic layer. (For interpretation of the references to colour in this figure legend, the reader is referred to the web version of this article.)

Table 3
Formation energy F (eV), diffusion barrier ΔE^{int} (eV), effective diffusion barriers ΔE^{eff} (eV), and their corresponding attempt-to-diffuse frequencies ν^{int} (THz), ν^{eff} (THz) for various inner-layer or inter-layer diffusion mechanisms. Each diffusion mechanism is related to a certain point defect.

Defects	F	Inner layer				Inter layer			
		ΔE^{int}	ν^{int}	ΔE^{eff}	ν^{eff}	ΔE^{int}	ν^{int}	ΔE^{eff}	ν^{eff}
I_i	1.01	0.14	0.73	1.88	0.36	0.24	1.71	1.98	0.85
I_{Zr}	− 0.73	3.36	0.83	3.36	0.41	3.36	0.83	3.36	0.41
$I_{Zr} - V_{Zr}$	0.83	0.54	1.68	2.09	0.84	0.74	2.18	2.30	1.09
$I_{2Zr} - V_{Zr}$	2.19	0.91	2.87	3.83	1.43	1.02	2.25	4.29	1.12

certain diffusion mechanism is a function of the defect formation energy, the diffusion energy barrier, and the vibration frequencies of the system (see Eqs. (4) and (8)). In Eq. (8), since the summation term in the denominator is a constant at a certain temperature, the two exponential terms in the numerator can be combined together as $exp\left(-\frac{\Delta E_i^{int}+F_i}{k_B T}\right)$. The effective diffusion barrier ΔE_i^{eff} is linearly proportional to $\Delta E_i^{int} + F_i$ (See Table 3) and the constant term is a normalizing factor. The formation energies, the effective diffusion barriers, and the corresponding vibration frequencies are listed in Table 3. Besides these parameters, the diffusion lengths (d_i) and the number of equal diffusion paths (n_i) in Eq. (6) together are used to calculate the diffusivity of the iodine diffusion in zirconium via various point defects.

The effective diffusion coefficients for the diffusion mechanisms listed in Table 3 are plotted in Fig. 7. The temperature ranges from 300 K to 2000 K. Different colors represent different diffusion mechanisms. For each diffusion mechanism, solid line represents the inter-layer diffusion and the dash line represents the inner layer diffusion. First of all, the iodine diffusion via interstitial diffusion site is the fastest diffusion mechanism. Both of the iodine interstitial mechanisms via inner layer channel or inter layer way are fast diffusion paths for iodine atoms diffusion in α−zirconium. On the contrary, the iodine diffusion rate is slowed down via the point defect of $I_{2Zr} - V_{Zr}$. That is, the vacancies are traps for the iodine atoms in α−zirconium and it results in the decrease of the diffusion rate of iodine in α−zirconium. Finally, the experimental data [8] matches the upper lines well. Since the fastest diffusion mechanism may dominate the diffusion process and it can be measured by the experimental methods. Recall the data in Table 3, although the formation energy of I_{Zr} is very low, its diffusion barrier is rather high. The formation energy and the diffusion barrier of $I_{2Zr} - V_{Zr}$ are both much higher than that of I_i and it makes the diffusion very slow. Because the formation energy of the defects and their diffusion barriers are at the same level and they can be both activated by thermal energy, both of the two parameters are important for the diffusion coefficient of iodine in zirconium.

From Eq. (9) at 400 °C (673 K) and 600 °C (873 K) the effective diffusion coefficient equals to $D = 5.20 \times 10^{-22} m^2 s^{-1}$and $9.95 \times 10^{-19} m^2 s^{-1}$. (see Table 4) Comparing to the experimental data from paper of Monocoffre [8], they get D equals $9 \times 10^{-22} m^2 s^{-1}$ and $7 \times 10^{-19} m^2 s^{-1}$. They are almost in the same order of our calculation results.

So the dominate diffusion mechanism are interstitial diffusion and the substitutional diffusion under the help of vacancy. And they might cause the major release path of iodine through Zr clad.

4. Conclusions

Iodine is one of the fission product of fuel in nuclear reactors. One main function of a cladding material is to prevent the fission products from releasing to the cooling water. Since neutron irradiation may generate complex point defects in the cladding material, iodine atom diffusion rates via complex point defects in the cladding material are calculated with first principles calculations and NEB diffusion path search calculations. Effective diffusion rate is used to evaluate the defect effect on iodine diffusion in Zr. Effective diffusion rate is determined by the formation energy, diffusion energy barrier, and vibration model.

Our calculations show that in the temperature range from 300 K to 2000 K, the iodine interstitial diffusion and the iodine diffusion via $I_{Zr} - V_{Zr}$ are the dominant diffusion mechanisms. Compared with the iodine interstitial diffusion, vacancies increase the effective barriers and slow down the effective diffusion coefficient. The vacancies may be traps for iodine diffusion. Especially, the point defect of $I_{2Zr} - V_{Zr}$ makes the iodine diffusion rather slow. Our calculated iodine diffusion coefficients agree with the experimental data well [8]. This indicates that bulk diffusion may be one main diffusion mechanism for the iodine diffusion in zirconium alloy.

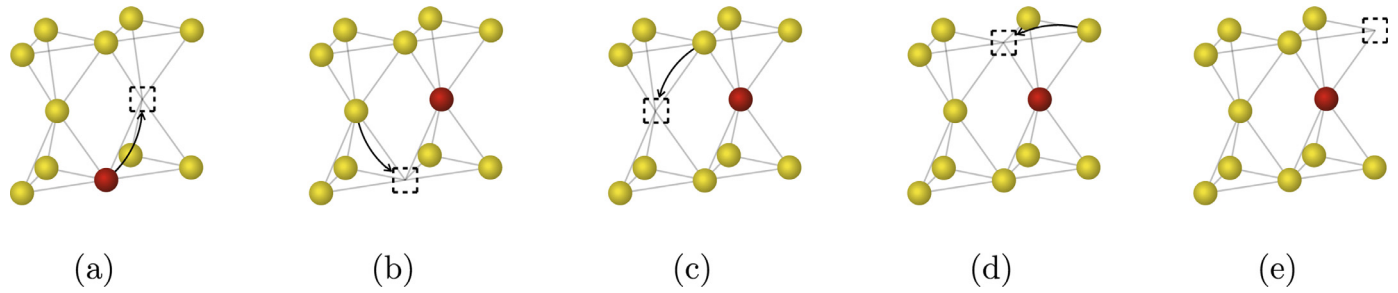

Fig. 5. Schematic of iodine diffusion with a vacancy nearby ($I_{Zr} - V_{Zr}$) in bulk zirconium. After diffusion, the iodine atom and the vacancy move to the upper atomic layer symmetrically. The yellow balls represent zirconium atoms and the red balls are iodine atoms. The dash squares are vacancies in the bulk zirconium. (For interpretation of the references to colour in this figure legend, the reader is referred to the web version of this article.)

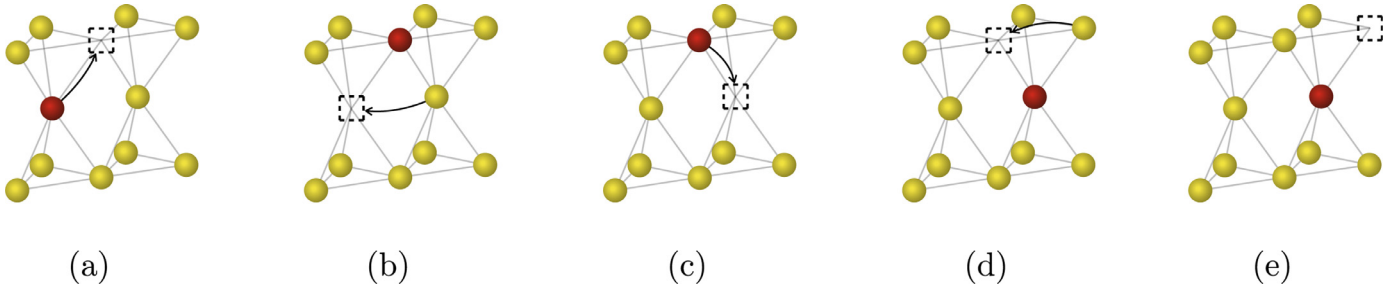

Fig. 6. Schematic of iodine diffusion with one vacancy nearby ($I_{Zr} - V_{Zr}$) between two atomic layers in bulk zirconium. The yellow balls are zirconium atoms, the red balls are iodine atoms. Dash squares are vacancies. (For interpretation of the references to colour in this figure legend, the reader is referred to the web version of this article.)

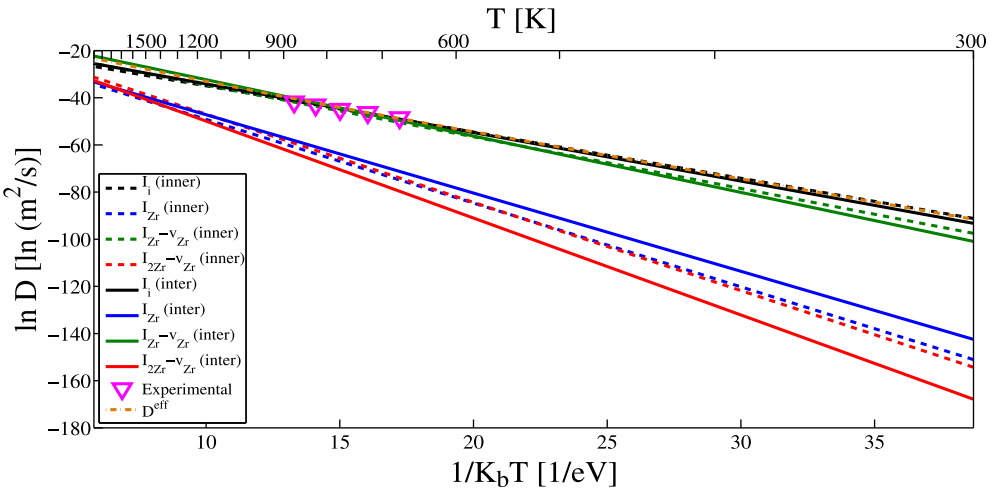

Fig. 7. Effective diffusion coefficients of iodine impurity in zirconium as a function of temperature for various diffusion mechanisms (calculated with Eq. (8)). The temperature ranges from 300 K to 2000 K. The purple triangles represent experimental data [8]. (∥ represents the diffusion along the $\vec{c}$ axis, ⊥ represents the diffusion perpendicular to the $\vec{c}$ axis.) . (For interpretation of the references to colour in this figure legend, the reader is referred to the web version of this article.)

Table 4
Comparing calculational and experimental results of diffusion coefficient.

Temperature	$D\,(m^2/s)$	
(K)	Experimental [8]	Calculated
673	9×10^{-22}	5.20×10^{-22}
723	8×10^{-21}	5.09×10^{-21}
773	3×10^{-20}	3.71×10^{-20}
823	2×10^{-19}	2.12×10^{-19}
873	7×10^{-19}	9.95×10^{-19}

Conflict of Interest

None.

Acknowledgments

This work is supported by National Science and Technology Major Project of China under contract No. 2015ZX06004001-002.

References

[1] C. Azevedo, Selection of fuel cladding material for nuclear fission reactors, Eng. Fail. Anal. 18 (8) (2011) 1943–1962.
[2] J.B. Malherbe, Diffusion of fission products and radiation damage in sic, J. Phys. D Appl. Phys. 46 (47) (2013) 473001.
[3] A. Garlick, P. Wolfenden, Fracture of zirconium alloys in iodine vapour. J. Nucl. Mater. 41 (3) (1971) 274–292.
[4] L. Brunisholz, C. Lemaignan, Iodine-induced stress corrosion of zircaloy fuel cladding: initiation and growth. Zirconium in the Nuclear Industry. (1987).
[5] P. Sidky, Iodine stress corrosion cracking of zircaloy reactor cladding: iodine chemistry (a review), J. Nucl. Mater. 256 (1) (1998) 1–17.
[6] B. Lewis, W. Thompson, M. Kleczek, K. Shaheen, M. Juhas, F. Iglesias, Modelling of iodine-induced stress corrosion cracking in candu fuel, J. Nucl. Mater. 408 (3) (2011) 209–223.
[7] J. Kalilainen, T. Kärkelä, R. Zilliacus, U. Tapper, A. Auvinen, J. Jokiniemi, Chemical reactions of fission product deposits and iodine transport in primary circuit conditions, Nucl. Eng. Des. 267 (2014) 140–147.
[8] N. Moncoffre, G. Carlot, A. Chevarier, Diffusion study of implanted iodine in zirconium using ion beams, Surf. Coat. Technol. 128 (2000) 9–14.
[9] L. Desgranges, C. Riglet-Martial, I. Aubrun, B. Pasquet, I. Roure, J. Lamontagne, T. Blay, Evidence of tellurium iodide compounds in a power-ramped irradiated {UO2} fuel rod, J. Nucl. Mater. 437 (2013) 409–414.
[10] E. Friedland, N. van der Berg, J. Malherbe, R. Kuhudzai, A. Botha, E. Wendler, W. Wesch, Study of iodine diffusion in silicon carbide, Nucl. Instrum. Methods Phys. Res. Sect. B 268 (2010) 2892–2896.
[11] A. Audren, A. Benyagoub, L. Thome, F. Garrido, Ion implantation of iodine into silicon carbide: influence of temperature on the produced damage and on the behaviour, Nucl. Instrum. Methods Phys. Res. Sect. B 266 (12) (2008) 2810–2813.
[12] E. Friedland, N. van der Berg, J. Malherbe, J. Hancke, J. Barry, E. Wendler, W. Wesch, Investigation of silver and iodine transport through silicon carbide layers prepared for nuclear fuel element cladding, J. Nucl. Mater. 410 (2011) 24–31.
[13] S. Dwaraknath, G. Was, The diffusion of cesium, strontium, and europium in silicon carbide, J. Nucl. Mater. 476 (2016) 155–167.
[14] S. Dwaraknath, G. Was, Radiation enhanced diffusion of cesium, strontium, and europium in silicon carbide, J. Nucl. Mater. 474 (2016) 76–87.
[15] P. Hohenberg, W. Kohn, Inhomogeneous electron gas, Phys. Rev. 136 (1964) B864–B871.
[16] E. Wimmer, R. Najafabadi, G.A. Young Jr, J.D. Ballard, T.M. Angeliu, J. Vollmer, J.J. Chambers, H. Niimi, J.B. Shaw, C. Freeman, et al., Ab initio calculations for industrial materials engineering: successes and challenges, J. Phys. 22 (38) (2010) 384215.
[17] M.L. Rossi, C.D. Taylor, First-principles insights into the nature of zirconium–iodine interactions and the initiation of iodine-induced stress–corrosion cracking, J. Nucl. Mater. 458 (2015) 1–10.
[18] M. Christensen, T. Angeliu, J. Ballard, J. Vollmer, R. Najafabadi, E. Wimmer, Effect of impurity and alloying elements on zr grain boundary strength from first-principles computations, J. Nucl. Mater. 404 (2) (2010) 121–127.
[19] M. Klipfel, P.V. Uffelen, Ab initio modelling of volatile fission products in uranium mononitride, J. Nucl. Mater. 422 (1–3) (2012) 137–142.
[20] S. Khalil, N. Swaminathan, D. Shrader, A.J. Heim, D.D. Morgan, I. Szlufarska, Diffusion of ag along σ3 grain boundaries in 3c-sic, Phys. Rev. B 84 (2011) 214104.
[21] J. Rabone, E. López-Honorato, P.V. Uffelen, Silver and cesium diffusion dynamics at the β-sic σ5 grain boundary investigated with density functional theory molecular dynamics and metadynamics, Phys. Chem. A 118 (2014) 915–926.

[22] D. Shrader, I. Szlufarska, D. Morgan, Cs diffusion in cubic silicon carbide, J. Nucl. Mater. 421 (1) (2012) 89–96.
[23] D. Shrader, S.M. Khalil, T. Gerczak, T.R. Allen, A.J. Heim, I. Szlufarska, D. Morgan, Ag diffusion in cubic silicon carbide, J. Nucl. Mater. 408 (3) (2011) 257–271.
[24] R. Rurali, E. Hernández, P. Godignon, J. Rebollo, P. Ordejón, First-principles studies of the diffusion of b impurities and vacancies in sic, Phys. Rev. B 69 (12) (2004) 125203.
[25] H. Ko, J. Deng, I. Szlufarska, D. Morgan, Ag diffusion in sic high-energy grain boundaries: kinetic monte carlo study with first-principle calculations, Comput. Mater. Sci 121 (2016) 248–257.
[26] J. Deng, D. Morgan, I. Szlufarska, Kinetic monte carlo simulation of the effective diffusivity in grain boundary networks, Comput. Mater. Sci 93 (2014) 36–45.
[27] J. Deng, H. Ko, P. Demkowicz, D. Morgan, I. Szlufarska, Grain boundary diffusion of ag through polycrystalline sic in {TRISO} fuel particles, J. Nucl. Mater. 467 (2015) 332–340. Part 1.
[28] H.H. Wu, D.R. Trinkle, Direct diffusion through interpenetrating networks: oxygen in titanium, Phys. Rev. Lett. 107 (2011) 045504.
[29] H.H. Wu, P. Wisesa, D.R. Trinkle, Oxygen diffusion in hcp metals from first principles, Phys. Rev. B 94 (2016) 014307.
[30] R. Han, L. Liu, R. Tu, W. Xiao, Y. Li, H. Li, D. Shao, Iodine atom diffusion in sic and zirconium with first-principles calculations, Nucl. Technol. 195 (2016) 192–203.
[31] C. Varvenne, O. Mackain, E. Clouet, Vacancy clustering in zirconium: an atomic-scale study, Acta Mater. 78 (2014) 65–77.
[32] C. Varvenne, O. Mackain, L. Proville, E. Clouet, Hydrogen and vacancy clustering in zirconium, Acta Mater. 102 (2016) 56–69.
[33] G.M. Hood, Point defect diffusion in α-zr, J. Nucl. Mater. 159 (1988) 149–175.
[34] G. Samolyuk, A. Barashev, S. Golubov, Y. Osetsky, R. Stoller, Analysis of the anisotropy of point defect diffusion in hcp zr, Acta Mater. 78 (2014) 173–180.
[35] W. Kohn, L.J. Sham, Self-consistent equations including exchange and correlation effects, Phys. Rev. 140 (1965) A1133–A1138.
[36] H. Jónsson, G. Mills, K.W. Jacobsen, Nudged Elastic Band Method for Finding Minimum Energy Paths of Transitions. World Scientific, 1998, p. 385.
[37] G. Henkelman, H. Jónsson, Improved tangent estimate in the nudged elastic band method for finding minimum energy paths and saddle points, J. Chem. Phys. 113 (2000) 9978.
[38] G. Henkelman, B.P. Uberuaga, H. Jónsson, A climbing image nudged elastic band method for finding saddle points and minimum energy paths, J. Chem. Phys. 113 (2000) 9901.
[39] G. Kresse, J. Hafner, *Ab initio* molecular dynamics for liquid metals, Phys. Rev. B 47 (1993) 558–561.
[40] G. Kresse, J. Hafner, *Ab initio* molecular-dynamics simulation of the liquid-metal – amorphous-semiconductor transition in germanium, Phys. Rev. B 49 (1994) 14251–14269.
[41] J. Du, B. Wen, R. Melnik, Mechanism of hydrogen production via water splitting on 3c-sics different surfaces: a first-principles study, Comput. Mater. Sci 95 (2014) 451–455.
[42] P.E. Blöchl, Projector augmented-wave method, Phys. Rev. B 50 (1994) 17953–17979.
[43] G. Kresse, D. Joubert, From ultrasoft pseudopotentials to the projector augmented-wave method, Phys. Rev. B 59 (1999) 1758–1775.
[44] J.P. Perdew, K. Burke, M. Ernzerhof, Generalized gradient approximation made simple, Phys. Rev. Lett. 77 (1996) 3865–3868.
[45] J.P. Perdew, K. Burke, M. Ernzerhof, Generalized gradient approximation made simple, Phys. Rev. Lett. 78 (1997). 1396–1396
[46] G. Kresse, J. Furthmüller, Efficiency of ab-initio total energy calculations for metals and semiconductors using a plane-wave basis set, Comput. Mater. Sci 6 (1996) 15–50.
[47] G. Kresse, J. Furthmüller, Efficient iterative schemes for *ab initio*total-energy calculations using a plane-wave basis set, Phys. Rev. B 54 (1996) 11169–11186.
[48] D. Shrader, S.M. Khalil, T. Gerczak, T.R. Allen, A.J. Heim, I. Szlufarska, D. Morgan, Ag diffusion in cubic silicon carbide, J. Nucl. Mater. 408 (2011) 257–271.
[49] Additional information on the VASP Transition State Theory code, 2014, (http://theory.cm.utexas.edu/vtsttools/download.html).
[50] G. Boisvert, L.J. Lewis, Self-diffusion on low-index metallic surfaces: ag and au (100) and (111), Phys. Rev. B 54 (1996) 2880–2889.
[51] G.H. Vineyard, Frequency factors and isotope effects in solid state rate processes, J. Phys. Chem. Solids 3 (1–2) (1957) 121–127.
[52] X. Hu, R. Tu, J. Wei, C. Pan, J. Guo, W. Xiao, Nitrogen atom diffusion into tio2 anatase bulk via surfaces, Comput. Mater. Sci 82 (2014) 107–113.
[53] R.J. Brog, G.J. Dienes, An Introduction to Solid State Diffusion, Academic Press Inc. (1988) 93–96.
[54] R. Tendler, C. Varotto, Diffusion in solids, J. Nucl. Mater. 54 (2) (1974) 212–216.
[55] A.S. Nowick, Diffusion in Crystal Solids, Academic Press Inc. (1984) 118.